CHEMISTRY
A European Journal

A Journal of
ChemPubSoc Europe

Accepted Article

Title: Metal-free photoinduced atom transfer radical polymerization for highly sensitive detection of lung cancer DNA

Authors: Qianrui Liu, Lihe Jian, Ruiqian Liu, Huaixia Yang, Jinming Kong, and Xueji Zhang

To be cited as: *Chem. Eur. J.* 10.1002/chem.201904271

Link to VoR: http://dx.doi.org/10.1002/chem.201904271

Supported by
ACES

WILEY-VCH

10.1002/chem.201904271

WILEY-VCH

FULL PAPER

Metal-free photoinduced atom transfer radical polymerization for highly sensitive detection of lung cancer DNA

Qianrui Liu,[a] Lihe Jian,[b] Ruiqian Liu,[a] Huaixia Yang,[b] Jinming Kong,*[a] Xueji Zhang[c]

Abstract: A convenient and sensitive detection of biomolecules is of great significance to disease diagnosis. In this work, a metal-free photoinduced atom transfer radical polymerization (photoATRP) via reductive quenching pathway as a novel strategy is applied to achieve lung cancer DNA detection. Thiolated PNA is exploited to specifically recognize target DNA, and the initiator of photoATRP is linked to electrode surface via phosphate-Zr^{4+}-carboxylate. Under the excitation of blue light, reductive quenching pathway is activated with eosin Y (EY) as photoredox catalyst and N,N,N′,N″,N′-pentamethyldiethylenetriamine (PMDETA) as electron donor, and numerous polymeric chains are formed. Under optimal conditions, the linear range of this strategy is from 0.1 pM to 10 nM (R^2=0.989) with limit of detection (LOD) of 1.4 fM (14 zmol in 10 μL). The various light source of photoATRP and simple operation endow this biosensor great potential for practical applications.

Introduction

Recently, the understanding of pathogens and disease states from molecular level has attracted extensive attention.[1] Among those biomolecules, nucleic acids are commonly investigated. The morbidity and mortality of lung cancer have been increasing fast in recent years, and lung cancer is one of the most dangerous malignant tumors to human health. However, the content of nucleic acids related to lung cancer is frequently at extremely low level in the early stages of lung cancer. The achievement of nucleic acids detection at low concentrations can enhance the survival rate of patients. Traditional methods are the gold standard, e.g., polymerase chain reaction (PCR), southern blot and polyacrylamide gel electrophoresis, while are usually high cost, time consuming and skilled labour.[2]

A lot of efforts have been made to improve the detection sensitivity of nucleic acids in the past decade. Numerous amplification techniques have been derived, such as enzymatic amplification,[3] nanotechnology[4-5] and polymeric materials.[6] Among them, point-of-care testing of nucleic acids can be realized via directly introducing polymeric materials to nucleic acids. Reversible-deactivation radical polymerization (RDRP) has been receiving extensive attention in the fields of polymer chemistry, material science and biological applications in recent years, benefiting from the predetermined molecular weight, well-defined polymers, narrow-molecular-weight distribution and tolerance to functional groups. [7-8]

ATRP is the most extensively explored strategy among RDRP by virtues of various commercially available initiators and catalysts.[7] Recently, amplified detection of biological molecules based on ATRP were reported in many researches.[1,9-12] However, in all reports one limitation about ATRP must be overcome, that is the usage of metal catalyst for maintaining a reasonable reaction rate.[8]

A metal-free photoinduced ATRP (photoATRP) can eliminate residual metal. Light-driven reactions are vital for the being of human on Earth.[13] Photocatalysis has been becoming a powerful mean to perform several organic reactions.[14-18] Recently, photoredox catalysts is widely investigated due to its strong oxidation and reduction of its excited state and poor oxidation and reduction in the ground state.[19-20] Thus, light-driven reactions can be precisely controlled by light via photoredox catalysts. Among the photoredox catalysts, eosin Y is a kind of well-known reducible dyes due to the halide substituents on the chromophoric structure.[21] The metal-free photoATRP possesses two photoredox catalytic cycles by means of single electron transfer, oxidative quenching pathway and reductive quenching pathway.[22-25] Compared with oxidative quenching pathway, the formation of excited state of photoredox catalysts needs lower energy in reductive quenching pathway.[26] To the best of our knowledge, photoATRP as a strategy to achieve amplified detection of biomolecules has never been reported.

Herein, a metal-free photoATRP strategy for lung cancer DNA amplification detection via reductive quenching pathway was first reported in this work. The cytokeratin (CYFRA21-1) is common biomarker of lung cancer, thus the gene sequence of CYFRA21-1 was employed as target DNA (tDNA) in our work. PNA was first modified onto Au electrode surface via Au-S bond to capture tDNA. Subsequently, the initiator was introduced to PNA/DNA heteroduplexes via phosphate-Zr^{4+}-carboxylate. Photoredox catalytic cycle, reductive quenching pathway, was activated under the irradiation of blue light, while metal-free photoATRP started and polymeric chains modified with electroactive probes were formed. The fabricated process of this DNA biosensor was illustrated in Scheme 1. More importantly, the sunlight also could activate the photoATRP, and this strategy held great potential in bioanalytical applications due to the low background signal, simplicity, cost effectiveness and environment friendly.

[a] Dr. Q. Liu, R. Liu, Prof. J. Kong
School of Environmental and Biological Engineering
Nanjing University of Science and Technology
Nanjing 210094, P. R. China.
E-mail: j.kong@njust.edu.cn
[b] L. Jian, Prof. H. Yang
Pharmacy College
Henan University of Chinese Medicine
Zhengzhou 450008, P. R. China.
[c] Prof. X. Zhang
School of Biomedical Engineering
Shenzhen University Health Science Center
Shenzhen, Guangdong 518060, P. R. China.

10.1002/chem.201904271

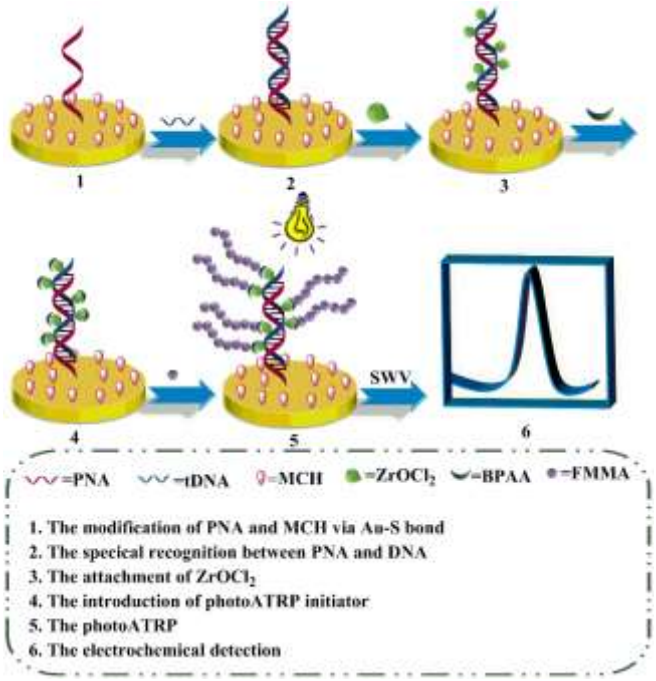

Scheme 1. The construction process of this DNA biosensor.

Results and Discussion

The mechanism of metal-free photoATRP.

In this work, metal-free photoATRP as a novel strategy was for the first time applied to achieve electrochemical lung cancer DNA detection. The mechanism of metal-free photoATRP based on reductive quenching pathway was illustrated in Scheme 2. The reductive quenching pathway started with photoexcitation, and the ground state of EY was transitted into excited state (EY*) by absorption photons. Subsequently, EY* was reduced to $EY^{\bullet-}$ via accepting electron from electron donor (D, PMDETA), meanwhile $D^{\bullet+}$ was generated. A reversible cycle of reductive quenching pathway to regulate ATRP was established based on the three forms of catalyst (EY, EY* and $EY^{\bullet-}$). $EY^{\bullet-}$ activated initiator of photoATRP (BPAA), and primary radicals ($P_0^{\bullet}$), halogen atom (X^-) and EY were formed. P_0• began to react with methacrylic monomers (M) to initiate the polymerization, and polymeric chains were generated, while P_n• participated with a process of electron transfer from X^- to $D^{\bullet+}$. Under the assistance of $D^{\bullet+}$, X^- was oxidated to halide radical to react with P_n• and deactivator (P_nX) was generated, at the same time, $D^{\bullet+}$ was reduced to D. The above reactions were repeated, and numerous monomers modified with electroactive probes were grafted on the electrode surface.

It's noteworthy that activation of ATRP only arises under excited state of catalyst in the light of dissociative electron-transfer (DET) theory.[7] EY would generate different electronic states under irradiation of the light. In Scheme 2, the ground state of EY was excited to form singlet excited state (^{1}EY*) by absorption photons. The electron spin flip of ^{1}EY* resulted in a change of ^{1}EY* multiplicity, that is called an intersystem crossing (ISC), and ^{1}EY* was turned into triplet excited state (^{3}EY*).[27] CV was applied to investigate the redox potentials of ground state of EY in 0.1M TBAP. As shown in FigS1, the oxidation potential of EY ($E_{EY^{\bullet+}/EY}$) was about +0.99 V vs SCE and the reduction potential of EY ($E_{EY/EY^{\bullet-}}$) was about -0.84 V vs SCE. The energy of ^{1}EY* (E_S) and ^{3}EY* (E_T) were respectively 53.16 kcal mol^{-1} (2.31 eV) and 44.0 kcal mol^{-1} (1.91 eV).[28] The redox potential of ^{1}EY* and ^{3}EY* was calculated according to the following equations:

$$E_{EY^{\bullet+}/^1EY^*} = E_{EY^{\bullet+}/EY} - E_S$$
$$E^1_{EY^*/EY^{\bullet-}} = E_{EY/EY^{\bullet-}} + E_S$$
$$E_{EY^{\bullet+}/^3EY^*} = E_{EY^{\bullet+}/EY} - E_T$$
$$E^3_{EY^*/EY^{\bullet-}} = E_{EY/EY^{\bullet-}} + E_T$$

The oxidation and reduction potential of ^{1}EY* ($E^1_{EY^*/EY^{\bullet-}}$ and $E_{EY^{\bullet+}/^1EY^*}$) were respectively 1.47 V and -1.32 V, and the oxidation and reduction potential of ^{3}EY* ($E^3_{EY^*/EY^{\bullet-}}$ and $E_{EY^{\bullet+}/^3EY^*}$) were 1.07 V and -0.92 V. Though the reduction potential of ^{1}EY* was more negative than that of ^{3}EY*, ^{3}EY* usually took part in the metal-free photoATRP because of its longer lifetime than ^{1}EY* ($\tau^1_{EY^*}$ = 2.1 ns, $\tau^3_{EY^*}$ = 24 μs).[29] The reduction potential of ^{3}EY* was -0.92 V which was more negative than alkyl bromide initiator (~-0.80 V vs SCE), however lifetime of ^{3}EY* was too short to reduce the initiator. Electron donor was necessary to quench ^{3}EY* for generating more stable state of EY ($EY^{\bullet-}$). Consequently, EY must be based on electron donor to activate polymerization based on reductive quenching pathway.

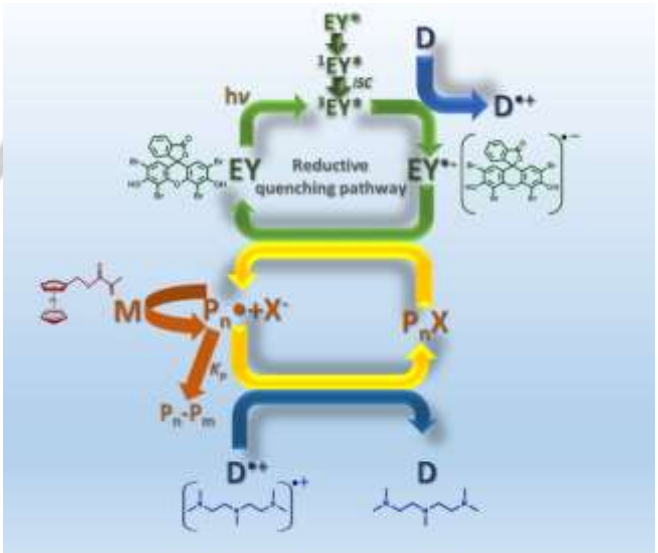

Scheme. 2 The mechanism of metal-free photoATRP.

The ultraviolet-visible spectroscopy of EY.

The photoexcitation of EY was the first step of metal-free photoATRP, the EY should process an apparent absorption in the

case of light irradiation. Therefore, the absorption regime of EY was investigated by ultraviolet-visible spectroscopy in mixture of DMSO and H_2O (1:1 in volume). As shown in Fig.1, 524 nm was the maximum absorption wavelength (λ_{max}) of EY (Fig.1a). The molar absorption coefficient is the light absorption capacity of chemical species at a given wavelength. The molar absorption coefficient of EY was calculated according to Beer-Lambert law (Eq. 1):

$$A=\varepsilon cL \quad (1)$$

where A is the absorbance, ε_{max} is the molar absorption coefficient at λ_{max}, c is the molar concentration of EY and L is the pathlength. The A was 0.508 which was seen from Fig.1, the molar concentration of EY was 10^{-5} M and the pathlength was 1.0 cm. The ε_{max} was 50800 M^{-1} cm^{-1}. As shown in Fig.1b, PMDETA had no effect on the process of photoexcitation of EY. In addition, PMDETA (Fig.1, c), FMMA (Fig.1, d) and BPAA (Fig.1, e) were all tested by ultraviolet-visible spectroscopy. None of them showed absorption, inditating negligible photochemical activity.

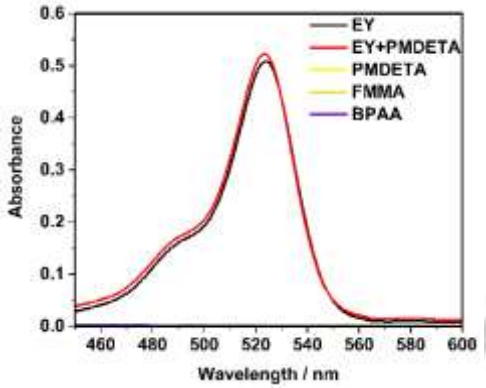

Figure.1 Ultraviolet-visible spectra of EY (10^{-5} M) (a), EY and PMDETA (1:2 in molarity, EY=10^{-5} M) (b), PMDETA (10^{-5} M) (c), FMMA (10^{-5} M) (d) and BPAA (10^{-5} M) (e) in mixture of DMSO and H_2O (1:1 in volume).

The surface coverage of PNA-modified Au electrode.

PNA is mimic of nucleic acid where negatively charged phosphate backbone of nucleic acid is replaced with a neutral protein-like backbone, and the neutral protein-like backbone alleviates the electrostatic repulsion of PNA/DNA heteroduplexes. Thus, the affinity of PNA/DNA heteroduplexes is stronger than DNA/DNA duplexes. Taking into account the affinity of PNA/DNA heteroduplexes, PNA was adopted as the capture probe for tDNA. Therefore, it was essential to investigate the surface coverage of PNA-modified Au electrode. Before calculating the surface coverage, the effective area of Au electrode (A_{eff}) was estimated. CV was utilized to evaluate A_{eff} in 5.0 mM $[Fe(CN)_6]^{3-}$ in 0.1 M KNO_3, according to (Eq. 2):

$$i=2.69\times10^5\times A_{eff}\times n^{2/3}\times D^{1/2}\times\vartheta^{1/2}\times C \quad (2)$$

where i is the anodic current of $[Fe(CN)_6]^{3-}$, n is the transferred electron number of $[Fe(CN)_6]^{3-}$, D is the diffusion coefficient of 5.0 mM $[Fe(CN)_6]^{3-}$ in 0.1 M KNO_3, υ is scan rate of CV and C represents the concentration of $[Fe(CN)_6]^{3-}$. As shown in Fig. S2, the value of i was acquired from cyclic voltammogram (FigS2, a), n is 1, the diffusion coefficient of 5.0 mM $[Fe(CN)_6]^{3-}$ in 0.1 M KNO_3 was 2.4×10^{-6} cm^2 s^{-1}.[30] The scan rate and the concentration of $[Fe(CN)_6]^{3-}$ were respectively 1.0 V s^{-1} and 5.0 mM. The A_{eff} was calculated to be about 0.054 cm^2. The number of repeative experiments is five.

The surface coverage (Γ) of PNA-modified Au electrode was determined according to the (Eq. 3):

$$\Gamma=Q/(nFA_{eff}) \quad (3)$$

where Q is consumed charge in CV and F is Faraday constant. F is 96485 C mol^{-1}. The ΔQ (ΔQ=0.067×10^{-5} C) was the Q difference of bare Au electrode and PNA-modified electrode obtained by CVs in 5.0 mM $[Fe(CN)_6]^{3-}$ in 0.1 M KNO_3 (FigS2. a, b). The value of Γ was calculated to be 1.3×10^{-10} mol cm^{-2}. In addition, the anodic current decreased after modifying PNA onto electrode surface because of the increased steric hindrance, suggesting that PNA was successful immobilized on the electrode surface.

The surface characterization of this biosensor.

AFM was applied to study morphology and surface roughness of the biosensor before and after the photoATRP on gold chip. The AFM images were shown in Fig.2. The surface high and surface roughness (R_a) of PNA/MCH/tDNA/Zr^{4+}/BPAA-modified gold chip were respectively 35.5 nm and 3.71 nm (Fig.2A). After the photoATRP, the surface high and R_a of gold chip increased to 40.2 nm and 3.98 nm (Fig.2B). The increase of surface high and R_a might be due to the polymeric chains produced by photo ATRP.

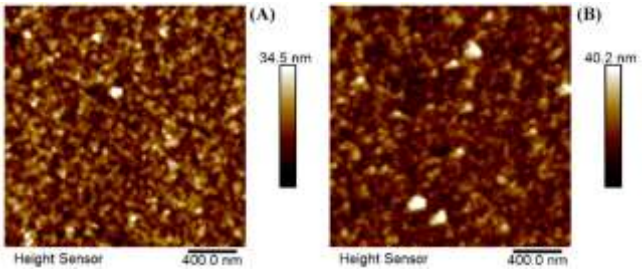

Figure.2 (A) The AFM images of gold chip before photoATRP. (B) The AFM images of gold chip after photoATRP.

Water contact angle (WCA) was applied to explore the hydrophilicity of the modified electrode. If the angle (θ) is greater than 90°, indicating that the surface is hydrophobic; if θ is less than 90°, the surface is hydrophilic, and smaller θ shows better hydrophilicity. As shown in Fig.S3, the θ of bare electrode was 94.55° because the surface of Au electrode was hydrophobic (Fig.S3, A). The θ decreased to 66.8° due to the hydrophilicity of amidogent of PNA (Fig.S3, B). After MCH was immobilized onto electrode surface, θ decreased to 49.3° (Fig.S3, C). This result was because lots of hydrophilic groups (hydroxyl) were introduced to electrode surface, indicating that MCH was successfully modified on the electrode surface. The θ further decreased to 47.2° due to the phosphate of tDNA, and this result

suggested the forming of PNA/DNA heteroduplexes (Fig.S3, D). If Zr^{4+} was added to biosensor, the θ increased to 62.2° (Fig.S3, E). Zr^{4+} was coordinated with phosphate of tDNA which led to the decrease of the hydrophilic groups (phosphate) exposed to the electrode surface, therefore the θ increased. The phenyl of BPAA was hydrophobic group, thus the θ increased to 64.9° after the attachment of BPAA (Fig.S3, F). After photoATRP, the θ decreased to 58.6° due to the hydrophilicity of methacrylates (Fig.S3, G).

Electrochemical characterizations.

SWV was utilized to evaluate the feasibility of this photoATRP biosensor in 1.0 M $LiClO_4$. The potential was from 0 V to 0.5 V. As shown in Fig.3A, if the electrochemical biosensor was in the presence of all the reagents, an obvious current was seen at the potential of 0.24 V (Fig.3A, a). Different substituents modified on the ring of cyclopentadiene will change the potential value of ferrocene. The electron withdrawing group will make the potential value of the ferrocene increase; the potential value of the ferrocene will decrease if the modified group is electron donating group. The potential value (0.24 V) was in the potential range of ferrocene.[31] If any of PNA (Fig. 3A, b), tDNA (Fig. 3A, c), Zr^{4+} (Fig. 3A, d) or BPAA (Fig. 3A, e) was not added into this biosensor, almost no peaks were observed. This was because that the initiator of photoATRP was disabled to introduce to electrode surface. Similarly, if EY (Fig.3A, f), PMDETA (Fig.3A, g) or light (Fig.3A, h) was absent from the biosensor, no peaks were seen which suggested that EY, electron donor (PMDETA) and light were indispensable during the photoexcitation of photoATRP. Likewise, If FMMA was absent of this biosensor, no peak was observed due to lack of the electroactive probes (Fig.3A,

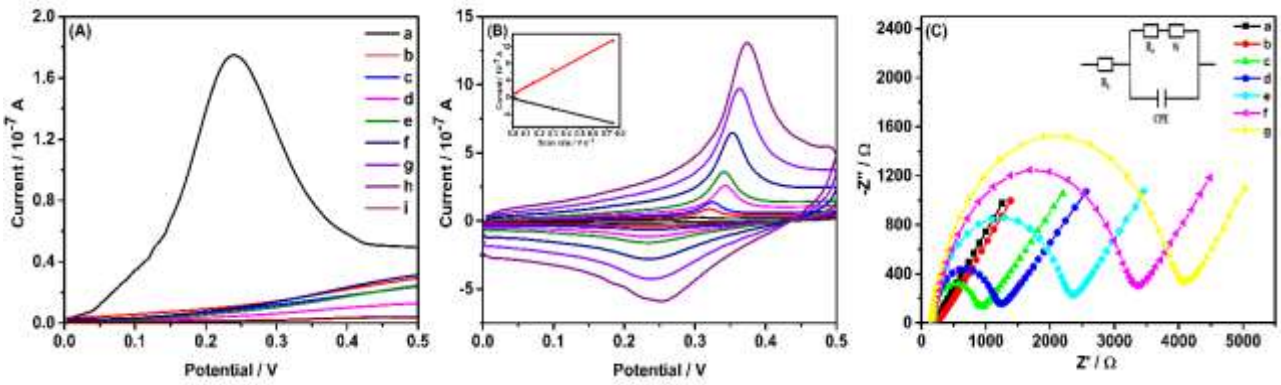

Figure.3 (A) SWVs of the PNA/MCH/tDNA/Zr^{4+}/BPAA/FMMA-modified electrode (a) and in the absence of PNA (b), tDNA (c), Zr^{4+} (d), BPAA (e), EY (f), PMDETA (g), light (h) or FMMA (i). (B) CVs of FMMA on the electrode surface at different scan rates in 1.0 M $LiClO_4$. Inset: The linear relationship between anode currents and cathode currents and scan rates. (C) The Nyquist plots of bare electrode (a), and PNA-modified electrode (b), PNA/MCH-modified electrode (c), PNA/MCH/tDNA-modified electrode (d), PNA/MCH/tDNA/Zr^{4+}-modified electrode (e), PNA/MCH/tDNA/Zr^{4+}/BPAA-modified electrode (f), PNA/MCH/tDNA/Zr^{4+}/BPAA/FMMA-modified electrode (g). Inset was the equivalent circuits.

i). Those results indicated that this strategy based on metal-free photoATRP was feasible.

CV with potential range from 0 V to 0.5 V was employed to characterize FMMA on the surface of the electrode at different scan rates in 1.0 M $LiClO_4$. As shown in Fig.3B, redox peak current presented a good linear relationship with different scan rates from 0.015 V s^{-1} to 1.0 V s^{-1}, indicating that this redox process was a surface controlled electrochemical quasi-reversible process. This result also suggested that FMMA was modified onto Au electrode surface via strong force instead of adsorption. In addition, the ratio of anode peak current and cathode peak current was greater than 1, which was because the complicated monolayer impended the transfer of electron.

EIS was applied to characterize the construction process of this electrochemical biosensor based on metal-free photoATRP in 5.0 mM $[Fe(CN)_6]^{3-/4-}$ in 0.1 M KNO_3 with a frequency range from 0.1 Hz to 100 kHz. In equivalent circuits inserted in Fig.3C, charge transfer resistance (R_{ct}), solution resistance (R_s), constant-phase element (CPE) and Warburg impedance (W) are commonly employed to describe impedance behavior. The semicircle at high frequency represents R_{ct}. As shown in Fig 3C, the bare Au electrode showed the smallest R_{ct} (~59.9 Ω) owing to fast electron transfer between the interface of electrode and solution (Fig.3C, a). The R_{ct} (~134 Ω) increased if PNA was added onto Au electrode due to the increased steric hindrance (Fig3C, b). After MCH was immobilized onto electrode surface, the R_{ct} (~733 Ω) further increased owing to ordered self-assembled molecular layer of MCH (Fig3C, c). The R_{ct} (~1050 Ω) gradually increased after tDNA was immobilized to the Au electrode surface (Fig3C, d). This result was mainly because the electrostatic repulsion between negatively charged phosphate backbone of tDNA and charge of $[Fe(CN)_6]^{3-/4-}$, and this result also suggested that tDNA successfully hybridized with PNA. When Zr^{4+} was attached to PNA/DNA heteroduplexe, the R_{ct} (~2170 Ω) further increased (Fig3C, e). Zr^{4+} led to the attachment of $[Fe(CN)_6]^{3-/4-}$ to PNA/DNA heteroduplexe via electrostatic attraction, and

subsequently electrostatic repulsion would be generated between the previously adsorbed $[Fe(CN)_6]^{3-/4-}$ and the $[Fe(CN)_6]^{3-/4-}$ in solution. Those reasons caused the increased of R_{ct}. After BPAA was introduced to electrode surface via phosphate-Zr^{4+}-carboxylate, the R_{ct} (~3160 Ω) continued to increase due to increased steric hindrance (Fig3C, f). The R_{ct} (~3910 Ω) further increased after metal-free photoATRP, suggesting that polymeric chains were successfully introduced this biosensor (Fig3C, g). The above results suggested that the modified process of the biosensor was opportune.

Optimization of conditions.

For realizing the best analytical performance of the strategy, it was essential to optimize conditions of photoATRP. The reductive quenching pathway was the precondition in this strategy, so the ratio of EY and PMDETA was optimized. The photoATRP cocktail contained 5 μL of 10 mM PMDETA. Before the ratio of EY and PMDETA was 0.5:1 (in molarity), the current signal increased with the decrease of EY observed from Fig.4A. This result was due to the formation of excessive excited state dimer (EY*), which was a famous phenomenon urged by high density of monomer in some specific chromophores.[32] After the ratio of EY and PMDETA was 0.5:1 (in molarity), the current signal decreased with the decrease of EY due to the slow kinetics seen from Fig.4A. Therefore, the optimal ratio of EY and PMDETA was 0.5:1.

In photoATRP, photons of blue light was driving force of polymerization. The number of photons (N) emitted per unit area and time by blue light was calculated according to (Eq.4):

$$I=Nhc/\lambda \quad (4)$$

where I is light intensity (4.0 mW cm^{-2}) measured at a distance of 10 cm along the emission axis, h is Planck constant (6.626×10^{-34} J•s), c is lightspeed (3×10^{8} m s^{-1}) and λ is wavelength of blue light (470 nm). N is calculated to be 9.46×10^{15}. According to Eq.4, the light intensity (I) is closely associated with the number of photons (N) emitted per unit area and time by blue light, and the light time of photoATRP was directly related to total of emission photons. The light intensity is stronger, the total number of photons is more during equal periods of time, and the light time of photoATRP is shorter. As shown in Fig.4B, the current signal of FMMA fast increased with increase of the reaction time before 180 min. Subsequently, the current signal slow increased, inditating that photoATRP approached photoATRP equilibrium under the reductive quenching pathway. Therefore, 180 min was selected as the optimal light time with total number of photons of 3.16×10^{18} received on the electrode surface.

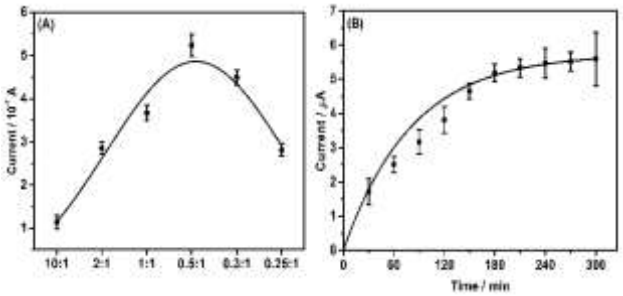

Figure.4 (A) The effects of different EY concentrations, and the ratio (in molarity) was EY: PMDETA (PMDETA: 5 μL, 10 mM; EY: 5 μL). (B) The effects of light time of photoATRP.

Analytical performance of this strategy.

To evaluate the analytical performance, SWV with potential range from 0 V to 0.5 V was applied to explore the relationship between tDNA concentrations and current signal in 1.0 $LiClO_4$ under optimal conditions. The current of FMMA increased with the increase of tDNA concentrations from 0.1 pM to 10 nM which was observed from Fig.5A. From calibration plots in Fig.5B, a good linear relationship was presented between the logarithm of different tDNA concentrations and current signal. The linear regression equation was I (10^{-7} A) = 1.99lg[tDNA/pM]+6.431 (R^2=0.989). The LOD was calculated to be 1.4 fM (S/N=3), and the minimum molar number of tDNA was calculated to be 14 zmol due to sample volume of 10 μL. As summarized in Table 1, the LOD was lower than many other strategies for ultrasensitive DNA detection. Numerous electroactive probes were introduced to electrode surface via photoATRP, which led to tremendous improvement of sensitivity. Metal-free photoATRP could solve the existing challenge of residual metal catalyst. Moreover, the light source of photoATRP was various, e.g. LED, Xenon lamp even sunlight. 0.1 pM tDNA was employed to evaluate the various light source. As shown in Fig. S4, the current signal was satisfactory under different light sources even the sunlight (under sunny weather in July in Zhengzhou (China)).

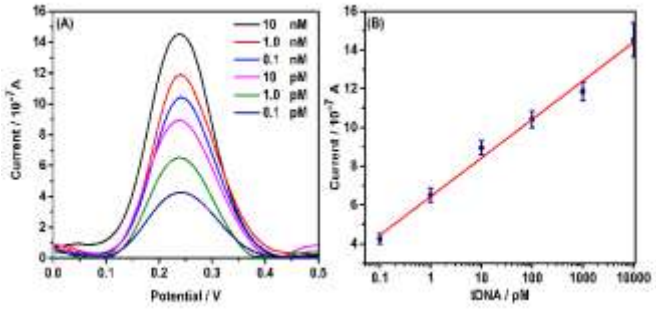

Figure 5. (A) SWVs of PNA/MCH/tDNA/Zr^{4+}/BPAA/FMMA-modified electrodes towards different tDNA concentrations in the range from 0.1 pM to 10 nM. (B) The calibration plots between the current signal of FMMA and the logarithm of tDNA concentrations.

10.1002/chem.201904271

Table 1. Comparison of this strategy with other strategies for ultrasensitive DNA detection.

Method	Linear range	LOD	Refs
Electrochemistry	0.1pM-0.1 nM	0.0403 pM	[33]
Fluorescence	0.5nM-50 nM	91 pM	[34]
Electrochemistry	0.01 pM-0.8 pM	4.16 fM	[35]
Electrochemistry	0.01pM-100 nM	30 fM	[36]
Fluorescence	20 fM-0.1 nM	20 fM	[37]
Fluorescence	not provided	13.5 fM	[38]
Electrochemistry	0.1pM-10 nM	1.4 fM	This work

Repeatability and stability of this biosensor.

To assess the repeatability of this biosensor based on photoATRP, seven repetitive intra-assays and inter-assays were respectively performed to detect 1.0 pM tDNA. The RSD of intra-assays and inter-assays were respectively 3.9% and 4.6%, indicating that the repeatability of this biosensor was satisfactory.

The PNA/MCH/tDNA/Zr^{4+}/BPAA/FMMA-modified electrodes were stored at a moisture saturated surroundings at 4 °C for two weeks, the recovery of current signal was 89.7%. This result implied that the stability of this biosensor was desirable.

Specificity and anti-interference of this method.

To evaluate the specificity of this strategy, SWV was applied to detect SBM, TBM and cDNA with potential range from 0 V to 0.5 V in $LiClO_4$. The concentrations of SBM, TBM and cDNA were all 0.1 pM. Under the same conditions, the current signal of 0.1 pM tDNA was compared with that of SBM, TBM and cDNA. As shown in Fig. 6A, the signal recovery of SBM and TBM were respectively 36.6% and 18.04%. The current signal of cDNA was close to background signal. The results was because that mismatched bases led to the unfavorable forming of PNA/DNA heteroduplexes according to the thermodynamics and the high specificity of PNA. The diminution of phosphate resulted in the decrease of initiator of photoATRP, therefore numerous monomer (FMMA) dramatically decreased. Those results evidenced that this strategy had high specificity.

The anti-interference of this strategy was assessed via using 1%, 5% and 10% normal human serum (NHS) as diluted solution of 0.1 pM tDNA. As shown in Fig.6B, the recovery of current signal in 1%, 5% and 10% serum samples were respectively 95.4%, 91.6%, 82.6%, indicating that this strategy showed a good anti-interference capability.

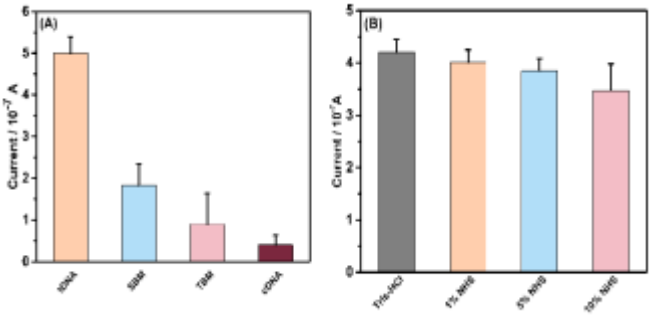

Figure 6. (A) SWV responses toward 0.1 pM tDNA, SBM, TBM and cDNA. (B) SWV responses of 0.1 pM tDNA in Tris-HCl, 1%, 5% and 10%NHS.

Conclusions

In conclusion, a novel electrochemical biosensor was firstly reported to achieve ultrasensitive detection of lung cancer DNA via metal-free photoATRP. The photoATRP was for the first time applied in the electrochemical biosensing for the detection of biomolecules. Moreover, the light source was various, even sunlight could also activate the polymerization. This strategy had the advantages of low background signal, simple preparation and cost effectiveness, those virtues endowed great potential for practical applications.

Experimental Section

The preparation of electrochemical biosensor.

Before the use of Au electrode, it needed to be pretreated.[1] The Au electrode was incubated in 10 μL of 0.5 μM PNA for 90 min at 37 °C to form a self-assembled monolayers (SAMs) via Au-S bond. After washing with Tris-HCl buffer, PNA-modified Au electrode was immersed into 400 μL of 5 mM MCH for 30 min at 37 °C, following by rinsing with 70% ethanol and ultrapure water. Afterwards, tDNA was added into electrode surface for 90 min at 37 °C, following by rinsing with Tris-HCl buffer. Then, the electrode was incubated in 400 μL of 5 mM $ZrOCl_2$ for 15 min at 37 °C. After washing with 10% ethanol and ultrapure water, Au electrode was incubated in 400 μL of 1 mM BPAA for 30 min at 37 °C. Then the Au electrode was rinsed with 15% ethanol and ultrapure water.

The above modified electrode was immersed into metal-free photoATRP cocktail and the cocktail was irradiated by 470 nm LED array at room temperature, and the illumination distance was 10 cm. After a given time, the PNA/MCH/tDNA/Zr^{4+}/BPAA/FMMA-modified electrode was washed with DMSO and ultrapure water to remove the adsorbed monomer. The chemical structures was shown as Fig.S5.

Finally, SWV was applied to record the current signal of FMMA in 1.0 M $LiClO_4$, and the potential was from 0 V to 0.5 V.

The other details of materials and apparatus could be found in Supplementary material.

Acknowledgements

Thanks for the National Natural Science Foundation of China (21974068).

Keywords: Metal-free photoinduced ATRP • reductive quenching pathway • lung cancer DNA • eosin Y

[1] Q. Hu, Q. W. Wang, G. Z. Sun, J. M. Kong, X. J. Zhang, *Anal. Chem.* **2017**, *89*, 9253-9259.

[2] S. Bi, S. Z. Yue, S. S. Zhang, *Chem. Soc. Rev*. **2017**, *46*, 4281-4298.

[3] Q. M. Shen, L. Han, G. C. Fan, J. R. Zhang, L. P. Jiang, J. J. Zhu, *Anal. Chem.* **2015**, *87*, 4949-4956.

[4] A. J. Cox, H. N. Bengtson, K. H. Rohdeb, D. M. Kolpashchikov, *Chem. Commun.* **2016**, *52*, 14318-14321.

[5] S. S. Liu, S. L. Zhao, W. W. Tu, X. Y. Wang, X. Wang, J. C. Bao, Y. Wang, M. Han, Z. H. Da, *Chem. Eur. J.* **2018**, *24*, 3677-3682

[6] Y. W. Peng, Y. Huang, Y. H. Zhu, B. Chen, L.Y. Wang, Z. C. Lai, Z. C. Zhang, M. T. Zhao, C. L. Tan, N. L. Yang, F. W. Shao, Y. Han, H. Zhang, *J. Am. Chem. Soc.* **2017**, *139*, 8698-8704.

[7] X. C. Pan, C. Fang, M. Fantin, N. Malhotra, W. Young So, L. A. Peteanu, A. A. Isse, A. Gennaro, P. Liu, K. Matyjaszewski, *J. Am. Chem. Soc.* **2016**, *138*, 2411-2425.

[8] D. Konkolewicz, K. Schröder, J. Buback, S. Stefan Bernhard, K. Matyjaszewski, *ACS Macro Lett.* **2012**, *1,* 1219-1223.

[9] Q. Hu, Q. W. Wang, J. M. Kong, L. Z. Li, X. J. Zhang, *Biosens. Bioelectron.* **2018**, *101*, 1-6.

[10] Q. R. Liu, K. F. Ma, D. X. Wen, Q. W. Wang, H. B. Sun, Q. Y. Liu, J. M. Kong, *J. Electroanal. Chem.* **2018**, *823*, 20-25.

[11] L. Yuan, W. Wei, S. Q. Liu, *Biosens. Bioelectron.* **2012**, *38*, 79-85.

[12] Y. F. Wu, W. Wei, S. Q. Liu, *Acc. Chem. Res.* **2012**, *45*, 1441-1450.

[13] N. Corrigan, J. Yeow, P. Judzewitsch, J. T. Xu, C. Boyer, *Angew. Chem.* **2019,** *131*, 5224-5243.

[14] J. C. Theriot, C. H. Lim, H. S. Yang, M. D. Ryan, C. B. Musgrave, G. M. Miyake, *Science* **2016**, *352*, 1082-1086.

[15] S. Almohammed, S. T. Barwich, A. K. Mitchell, B. J. Rodriguez, J. H. Rice, *Nat. Commun.* **2019**, *10*, 1-11.

[16] T. G. Ribelli, M. Fantin, J. C. Daran, K. F. Augustine, R. Poli, K. Matyjaszewsk, *J. Am. Chem. Soc.* **2018**, *140*, 1525-1534.

[17] C. L. Hao, L. G. Xu, M. Z. Sun, H. Y. Zhang, H. Kuang, C. L. Xu, *Chem. Eur. J.* **2019**, *25*, 1-7.

[18] V. Hilberg, O. Avrutina, A. Ebenig, D. Yanakieva, T. Meckel, M. Biesalski, H. Kolmar, *Chem. Eur. J.* **2019**, *25*, 1746-1751.

[19] C. A. Figg, J. D. Hickman, G. M. Scheutz, S. Shanmugam, R. N. Carmean, B. S. Tucker, C. Boyer, B. S. Sumerlin, *Macromolecules* **2018**, *51*, 1370-1376.

[20] J. Yeow, R. Chapman, J. T. Xu, C. Boyer, *Polym. Chem.* **2017**, *8*, 5012-5022.

[21] A. U. Meyer, K. Strakova, T. Slanina, B. Koenig, *Chem. Eur. J.* **2016**, *22*, 8694-8699.

[22] C. J. Wallentin, J. D. Nguyen, P. Finkbeiner, C. R. J. Stephensonm, *J. Am. Chem. Soc.* **2012**, *134*, 8875-8884.

[23] J. D. Nguyen, J. W. Tucker, M. D. Konieczynska, C. R. J. Stephenson, *J. Am. Chem. Soc.* **2011**, *133*, 4160-4163.

[24] N. Corrigan, S. Shanmugam, J. T. Xu, C. Boyer, *Chem. Soc. Rev.* **2016**, *45*, 6165-6212.

[25] X. D. Liu, L. F. Zhang, Z. P. Cheng, X. L. Zhu, *Polym. Chem.* **2016**, *7*, 689-700.

[26] C. Bian, Y. N. Zhou, J. K. Guo, Z. H. Lu, *Macromolecules* **2018**, *51*, 2367−2376.

[27] D. P. Hari, B. König, *Chem. Commun.* **2014**, *50*, 6688-6699.

[28] T. Shen, Z. G. Zhao, Q. Yu, , H. J. Xu, *J. Photochem. Photobiol. A Chem.* **1989**, *47*, 203-212.

[29] N. A. Romero, D. A. Nicewicz, *Chem. Rev.* **2016**, *116*, 10075-10166.

[30] C. A. Schroll, S. Chatterjee, W. R. Heineman, S. A. Bryan, *Anal. Chem.* **2011**, *83*, 4214–4219.

[31] G. D. Liu, J. Wang, D. S. Wunschel, Y. H. Lin, *J. Am. Chem. Soc.* **2006**, *128*, 12382-12383.

[32] C. Kutahya, F. S. Aykac, G. Yilmaz, Y. Yagci, *Polym. Chem.* **2016**, *7*, 6094-6098.

[33] H. Y. Huang, W. Q. Bai, C. X. Dong, R. Guo, Z. H. Liu, *Biosens. Bioelectron.* **2015**, *68*, 442-446.

[34] H. Z. Zhao, J. J. Dong, F. L. Zhou, B. X. Li, *Microchim. Acta* **2015**, *182,* 2495-2502.

[35] E. H. Xiong, X. H. Zhang, Y. Q. Liu, J. W. Zhou, P. Yu, X. Y. Li, J. H. Chen, *Anal. Chem.* **2015**, *87*, 7291-7296.

[36] B. B. Kou, Y. Q. Chai, Y. L. Yuan, R. Yuan, *Anal. Chem.* **2018**, *90*, 10701-10706

[37] S. F. Liu, C. B. Cheng, T. Liu, L. Wang, H. W. Gong, F. Li, *Biosens. Bioelectron.* **2015**, *63*, 99-104.

[38] M. Z. Li, F. He, Q. Liao, J. Liu, L. Xu, L. Jiang, Y. L. Song, S. Wang, D. B. Zhu, *Angew. Chem. Int. Ed.* **2008**, *47*, 7258-7262.

10.1002/chem.201904271

WILEY-VCH

Entry for the Table of Contents

FULL PAPER

Metal-free photoinduced ATRP (photoATRP) via reductive quenching pathway as a novel strategy is applied to achieve lung cancer DNA electrochemical detection. To the best of our knowledge, photoATRP as a strategy to achieve amplified detection of biomolecules has never been reported.

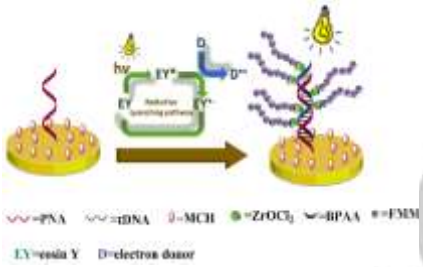

Qianrui Liu, Lihe Jian, Ruiqian Liu, Huaixia Yang, Jinming Kong, Xueji Zhang*

Page No.1 – Page No.7

Metal-free photoinduced atom transfer radical polymerization for highly sensitive detection of lung cancer DNA